energies

MDPI

Article

Improvement and Validation of the System Analysis Model and Code for Heat-Pipe-Cooled Microreactor

Li Ge [1], Huaqi Li [1,2]*, Xiaoyan Tian [2], Zeyu Ouyang [1], Xiaoya Kang [2], Da Li [2], Jianqiang Shan [1] and Xinbiao Jiang [2]

[1] School of Nuclear Science and Technology, Xi'an Jiaotong University, 28 Xianning West Road, Xi'an 710049, China; lihq561@163.com (H.L.); oyzy1998@stu.xjtu.edu.cn (Z.O.); jqshan@mail.xjtu.edu.cn (J.S.)

[2] Northwest Institute of Nuclear Technology, 28 Pingyu Road, Xi'an 710024, China; tianxiaoyan@nint.ac.cn (X.T.); kangxiaoya@nint.ac.cn (X.K.); lida@nint.ac.cn (D.L.); jiangxinbiao@nint.ac.cn (X.J.)

* Correspondence: gelili@mail.xjtu.edu.cn

Abstract: Heat-pipe-cooled microreactors (HPMR) use a passive high-temperature alkali metal heat pipe to directly transfer the heat of solid core to the hot end of the intermediate heat exchanger or thermoelectric conversion device, thus avoiding a single point failure. To analyze and evaluate the transient safety characteristics of an HPMR system under accident conditions, such as heat pipe failure in the core or a loss of system heat sink and other accidents, a previously developed model for transient analysis of a heat-pipe-cooled space nuclear reactor power system (HPSR) was improved and validated in this study. The models improved mainly comprise: (1) An entire 2-D solid-core heat transfer model is established to analyze the accident conditions of core heat pipe failure and system heat sink loss. In this model, radial and axial Fourier heat conduction equations are used to divide the core into *r*-θ direction control volumes. The physical parameters of the material in the control volume are calculated according to the volume-weighted average. (2) By coupling the heat transfer limit model and the two-dimensional thermal resistance network model, the transient model of a heat pipe for HPMR system analysis is improved. (3) Conversion system models are established to simulate the system characteristics of the advanced HPMR concept, such as thermoelectric conversion, Stirling conversion, and the open Brayton conversion analysis model. Based on the improved models, the HPMR system analysis program TAPIRSD was developed, which was verified by experimental data of the separated conversion components and the ground nuclear test device KRUSTY. The maximum deviation of the power output predicted by the energy conversion model is less than 8%. The accident conditions of the KRUSTY tests, such as load change, core heat pipe failure, and heat sink loss accident, were studied by using TAPIRSD. The results show that the simulation results of the TAPIRSD code agree well with the experimental data of the KRUSTY prototype reactor. The maximum error between the TAPIRSD code prediction and the measured value of the core temperature under accident conditions is less than 10 K, and the maximum deviation is less than 2%. The results show that the developed code can predict the transient response process of the HPMR system well. At the same time, the accuracy and reliability of the improved model are proved. The TAPIRSD is suitable for system transient analysis of different types of HPMRs and provides an optional tool for the system safety characteristics analysis of HPMR.

Keywords: heat-pipe-cooled microreactor; solid-core heat transfer model; conversion system model; TAPIRSD code; KRUSTY experiment

Citation: Ge, L.; Li, H.; Tian, X.; Ouyang, Z.; Kang, X.; Li, D.; Shan, J.; Jiang, X. Improvement and Validation of the System Analysis Model and Code for Heat-Pipe-Cooled Microreactor. *Energies* **2022**, *15*, 2586. https://doi.org/10.3390/en15072586

Academic Editor: Sung Joong Kim

Received: 22 February 2022
Accepted: 30 March 2022
Published: 1 April 2022

1. Introduction

To find a versatile and reliable solution to specialized power supply challenges involving military and civilian applications, such as high-power communication stations,

forward or remote operating bases, isolated microgrid communities, expeditionary or permanent military bases, and off-shore isolated platforms, the nuclear industry and research institutes worldwide are developing multiple reactor concepts with very small power for potential noncommercial or commercial purposes. These reactor concepts include the heat-pipe-cooled reactor (MegaPower system [1]), gas-cooled reactor (Holos system [2]), and liquid-metal-cooled reactor (SSTAR system [3]) designs, and are generally defined as miniature nuclear reactors or microreactors. This means the system is very simple, compact, and capable of producing heat energy of 1–20 MW for a heating supply or thermoelectric conversion [4]. As a result, the microreactor has the features of factory manufacturing, transportability, and adaptive adjustment. In addition, it has advantages over conventional reactors of microportability, simple design, and fast field installation, which make the microreactor a good solution to meet specialized power supply needs while considering environmental and climate problems.

Among the microreactor conceptual designs, the heat-pipe-cooled microreactor (HPMR) uses liquid metal heat pipes to transfer the reactor core heat directly to the hot end of the intermediate heat exchanger or thermoelectric conversion device under all normal and off-normal conditions. It also removes redundant heat passively after reactor shutdown. In addition, the heat pipe characteristics of design simplicity, modularity, and integration flexibility make a very small reactor core possible. The heat pipes can provide passive cooling without pumps, valves, or primary loop piping, thus avoiding the loss-of-coolant accident conditions found in commercial reactors. In summary, the HPMR makes full use of the excellent properties of heat pipes as they are used in other areas [5–7], such as heat exchangers, and solar and cryogenic systems. Thus, the HPMR has the advantages of high-temperature operation, the avoidance of a single point of failure, a compact system, and a more mature technology than other concepts. For example, the MegaPower microreactor developed by the LANL Laboratory is expected to undergo prototype verification in 2025, while the Kilopower space heat pipe reactor (HPR) [8] developed by NASA underwent ground verification testing in 2018. The eVinci HPMR concept [9], proposed by Westinghouse, has been used for special purposes. Therefore, the HPMR has become the most promising microreactor technology for advanced small nuclear reactors.

Taking the design of the eVinci HPMR as an example (Figure 1), HPMR mainly comprises an integrated solid core matrix with several high-temperature heat pipes (HTHPs), a primary heat exchanger, an energy conversion device, a decay heat removal system, and a control system. First, the reactor core HTHPs of the HPMR transfers the heat generated in the fuel to the hot end of the primary heat exchanger. Thereafter, heat from the heat pipe is transferred to the energy conversion device by the primary heat exchanger and converted into electricity at the end. There is no need for a pump to drive the continuous vapor/liquid internal flow at low pressure in the heat pipe, which makes heat pipes suitable for microreactors, with a maximum power of as much as several megawatts. Experimental results have shown that the power of a sodium heat-pipe-cooled space reactor can reach 100 kWe [10]. This is mainly based on robustness and low technical risk to ensure the high reliability and safety of space exploration.

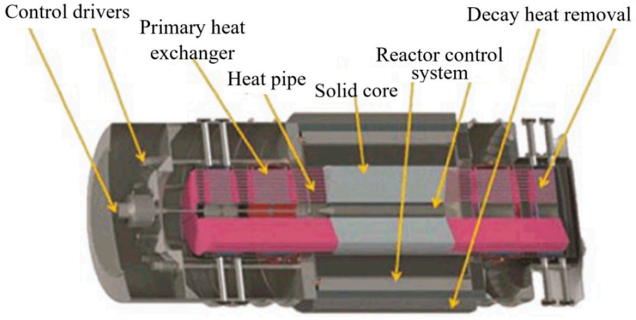

Figure 1. Layout of Westinghouse eVinci HPMR [10].

HPMR utilizes passive safety systems, such as heat pipes, instead of many specialized operators to prevent reactor overheating or meltdown. To determine the system transient safety characteristics of the HPMR and obtain the permission of the regulatory authorities, it is necessary to carry out a strict system safety assessment to analyze its safety characteristics under all normal and off-normal design conditions. Therefore, it is essential to develop a system analysis model and code for HPMR, such as the PKHP1D [11] code for heat transfer analysis of the SAFE-300 HPSR core, the FRINK code [12] for transient analysis of heat-pipe-cooled reactors, and the TAPIRS [13] code for the system transient analysis of the alkali metal thermal-to-electric conversion (AMTEC) HPSR.

However, these codes and models have some shortcomings in analyzing core heat transfer, heat pipe transients, and energy conversion characteristics. For example, in all these specifications, the core heat transfer model only uses the heat transfer model of the fuel rod. They can only simulate heat transfer from one fuel pin to a single heat pipe. These models cannot analyze the radial heat conduction characteristics of the system in a heat-sink-loss accident. In addition, the transient model of the core heat pipe cannot simulate the startup characteristics from the frozen state or the heat transfer limit of a heat pipe. These characteristics are very important for accurately predicting the transient heat transfer capability of heat pipes [14]. The PKHP1D and FRINK codes for heat pipe models are the traditional equivalent thermal resistance lumped parameter heat transfer model, which cannot analyze the HPMR system startup transient process. The heat pipe model of the TAPIRS code cannot analyze the heat transfer limits of heat pipes. The heat transfer limit of HTHPs directly affects the design and safety characteristics of HPMR [15]. Although some researchers have established the transient analysis model of HTHP in recent years and considered the heat transfer limit of heat pipe, they use CFD modeling [16] or two-dimensional finite element method [17]. Because these models require many numerical iterations, they are not suitable for transient analysis of HPMR. A transient model of the core heat pipe suitable for HPMR system characterization should be developed [18]. In addition, the PKHP1D code and FRINK code do not model the energy conversion system, while the TAPIRS code can only analyze AMTEC systems. The lack of an energy conversion model makes it impossible for existing codes to analyze new HPMR conceptual designs, such as the heat-pipe-segmented thermoelectric module conversion (HP-STMC) [19] with thermoelectric conversion, MegaPower reactor with open Brayton cycle conversion, and Kilopower with Stirling conversion [20]. On the other hand, these codes and models are not validated by the actual experimental data of the HPR system. Fortunately, the experimental data of the prototype reactor KRUSTY (Kilowatt Reactor Using Stirling Technology) system for the Kilopower HPR have been published [21,22], which provides a powerful reference for verifying system analysis models and codes of HPMRs.

In order to analyze and evaluate the transient safety characteristics of an HPMR under accident conditions, such as the core heat pipe failure or the loss of the system heat sink, the previously developed model and the transient analysis code TAPIRS for HPSRs were improved in this study. The improved model mainly comprises the following: (1) an entire solid-core heat transfer model, which is used to analyze the accident conditions of core heat pipe failure and system heat sink loss; (2) an improved heat pipe transient system analysis model for HPMRs developed by coupling the heat transfer limit model with a 2-D thermal resistance network model; and (3) conversion system models, including thermoelectric conversion, Stirling conversion, and the open Brayton conversion analysis model, which are used to simulate the system characteristics of advanced HPMR concept. Based on the improved models, the HPMR system analysis code TAPIRSD was also developed. In addition, the TAPIRSD code for the HPMR was validated by using the experimental data of the prototype reactor KRUSTY. The transient response of the KRUSTY reactor under accident conditions, such as load change, core heat pipe failure, and loss of heat sink accident, were simulated and analyzed by using the TAPIRSD code. The predicted results of the TAPIRSD code are compared with the experimental data of the KRUSTY prototype reactor.

2. Improvement of Model HPMR

2.1. Introduction of TAPIRS Code

The TAPIRS code [23] was developed to analyze and evaluate the transient safety response characteristics of a heat-pipe-cooled space reactor power system. It is preliminarily verified using the steady-state design parameters of the SAIRS concept [24] and relevant subcomponents. The models used in the TAPIRS code mainly comprise the point reactor kinetics model, uranium nitride (UN) fuel pin heat conduction model, heat pipe heat transfer model, AMTEC conversion model, and radiator heat transfer model, as shown in Figure 2.

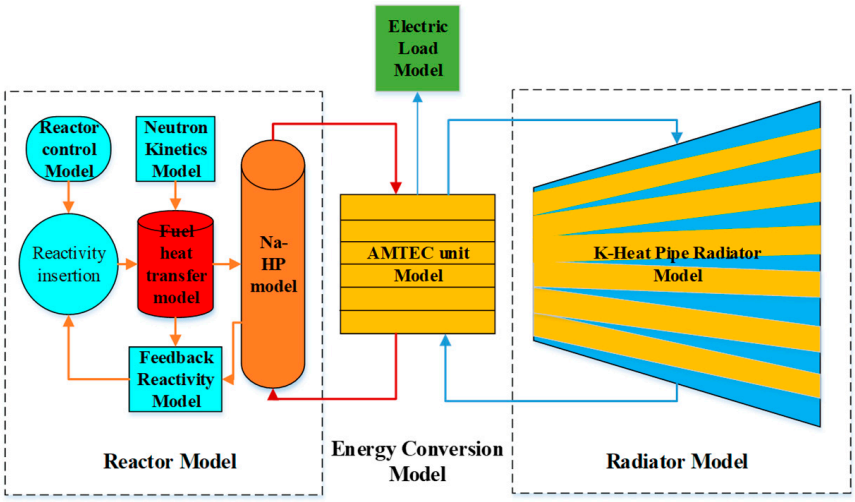

Figure 2. Schematic of the TAPIRS code.

The point reactor kinetics model was used to calculate the transient power of the reactor. The temperature negative feedback and the Doppler feedback effect of the fuel are considered in the model. The lumped parameter method was used to calculate the temperature of UN fuel rod. Assuming that the axial heat conduction in the UN fuel rods can be ignored, the radial heat conduction is axisymmetric. However, the UN fuel pin model can only simulate the heat transfer from one fuel pin to a single heat pipe, but cannot analyze the radial heat conduction characteristics of the core. Therefore, the TAPIRS code cannot be used to analyze the failure of heat pipes and loss of heat sink accidents in HPMR. The transient model of the heat pipe is used to simulate the transient process of heat pipe startup from a frozen state and normal transient process of the reactor heat pipe. It mainly comprises the thermal resistance network model and flat-front startup model. However, this model does not take into account the heat transfer limit of the heat pipe during startup and the normal transient, which has an important influence on the transient response characteristics of HPMR. The AMTEC conversion model is used to calculate the heat transfer and volt–ampere characteristics of the conversion device during the accident process. However, the energy conversion models of TAPIRS are only for AMTEC, and the lack of other types of models for energy conversion analysis limits the ability of TAPIRS to analyze other HPMR conceptual designs, such as the MegaPower reactor with open Brayton cycle conversion, Kilopower with Stirling conversion, and heat-pipe-segmented thermoelectric module conversion (HP-STMC) with thermoelectric conversion.

The TAPIRS code can be used to analyze various steady-state and transient conditions, including startup process, area loss of the heat pipe radiator, failure of the AMTEC module, and failure accident of the control drum. According to the analysis and evaluation results of the HPMR system characteristics, some models used in the TAPIRS code are neither accurate nor sufficiently comprehensive, and need to be further optimized and improved. (1) The heat transfer model of the fuel rod is approximately unreasonable. The analysis model of the radial heat transfer and equivalent heat transfer coefficient between the fuel

pin and heat pipe is insufficient, which means that the heat pipe failure accident cannot be accurately simulated by TAPIRS. (2) The heat transfer limit of the heat pipe is not considered in the heat pipe transient analysis model, but the heat transfer limit determines the response characteristics in some accidents and affects the safety of the HPMR system. (3) The energy conversion model is not sufficiently comprehensive to cover the conversion system commonly used in existing HPMR designs, such as thermoelectric conversion, open Brayton cycle conversion, Stirling conversion, and so on, which limits the universality of the TAPIRS code. (4) Using the concept of SAIRS and the steady-state design parameters of related subcomponents, the code is preliminarily verified. It is necessary to further use the experimental data of the reference heat pipe reactor for verification. Aiming at these problems, the transient models of core heat transfer and the heat pipe are improved, and an analysis model suitable for different energy conversion systems are established. Then, the experimental data of the prototype reactor KRUSTY are used to verify the TAPIRSD code for the HPMR based on the improved model. The improvement of those models is introduced in the following sections.

2.2. Core Heat Transfer Model

The TAPIRS code previously developed can only simulate heat transfer from a fuel pin to a single heat pipe, and its equivalent method has limitations. For example, the change in heat transfer coefficient at the interface between fuel cladding and the heat pipe wall is not taken into account. It is impossible to simulate the radial heat transfer across the entire core. Therefore, it is impossible to simulate the accident conditions of heat pipe failure and heat sink loss. As a result, the core heat transfer model of the HPMR was improved in this study.

2.2.1. Solid-Core Heat Transfer Model

HPMR is usually designed with an all-solid core. Under normal operating conditions, the heat of core fuel can only be transferred through heat pipes. However, when a small number of heat pipe failure accidents occur, the radial power distribution is uneven. In addition, the decay heat removal of most HPMRs under loss-of-coolant accidents depends on the radial heat conduction from the core to the radial reflector. Therefore, by dividing the HPMR core into different control volumes along the radial direction and circumferential directions, a two-dimensional radial heat conduction model is established, and the heat source term of the heat pipe in the volumes shown in Figure 3 is considered. The 2-D heat conduction equation of the entire core along the radial and circumferential directions can be solved using the finite difference method. The average core temperature can be calculated as follows:

$$\rho C_p V \frac{dT}{dt} = \frac{V}{r}\frac{\partial}{\partial r}\left(rk\frac{\partial T}{\partial r}\right) + \frac{V}{r}\frac{\partial}{\partial \theta}\left(\frac{k}{r}\frac{\partial T}{\partial \theta}\right) + q_f + q_{hp} \quad (1)$$

$$q_{hp} = N h_{hp} A_e \left(T - T_{hpe}\right) \quad (2)$$

where ρ is the equivalent density of the calculation region (kg/m^3); C_p is the equivalent specific heat (J·kg^{-1}·K^{-1}); V is the volume (m^3); T is the mean temperature of the calculation region (K); r is the equivalent radius (m); k is the equivalent thermal conductivity of the calculation region (W/(m·K)); q_f is the core thermal power (W); q_{hp} is the heat transferred power by the core heat pipe (W); N is the number of heat pipes in the calculation region; h_{hp} is the equivalent heat transfer coefficient at the interface of UN fuel cladding and heat pipe (W/(m^2·K)), which can be calculated using the equivalent heat transfer coefficient model in Section 2.2.3; A_e is the heat transfer area (m^2); and T_{hpe} is the heat pipe evaporation section wall temperature (K), which can be calculated using the heat pipe transient model.

The equivalent physical parameters of the material in the control volume are calculated according to the volume-weighted average:

$$\rho = \sum_{1}^{n} f_i \rho_i,\ C_p = \frac{\sum_{1}^{n} f_i \rho_i C_i}{\rho},\ k = \sum_{1}^{n} f_i k_i \tag{3}$$

where f_i is the volume fraction of material i; ρ_i is the density of material i (kg/m^3); C_i is the specific heat of material i (J·kg^{-1}·K^{-1}); and k_i is the thermal conductivity of material i (W/(m·K)).

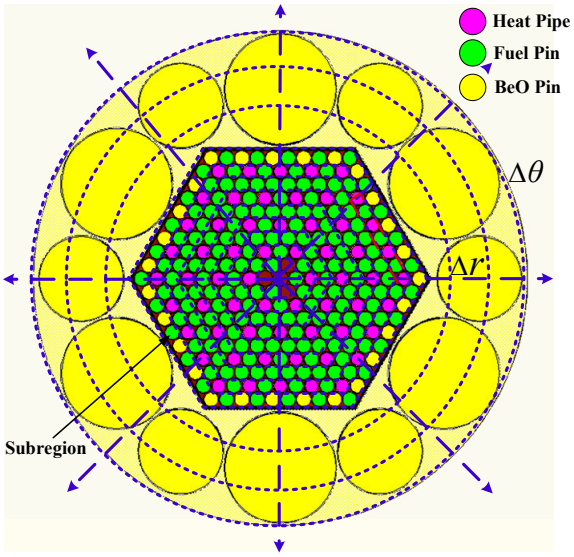

Figure 3. Schematic of 2-D heat conduction model in the HPMR core.

The boundary condition of the radial reflector is given by:

$$-k\frac{\partial T}{\partial r}\bigg|_{r=r_{ref}} = h_b(T - T_a) \tag{4}$$

where h_b is the heat transfer coefficient (W/(m^2·K)) and T_a is the space temperature (K).

2.2.2. Fuel Assembly Heat Transfer Model

The HPMR core has various heat pipe fuel assembly layout designs, but there is a certain proportion between the number of fuel rods and heat pipes (e.g., 3:1 for the SAIRS concept, 1:1 for MegaPower, and 6:1 for SAFE), and the hexagonal core layout is used most in HPMRs. The heat transferred from the fuel pellet to the outer wall of the heat pipe passes through three layers of solid material: fuel pellet, cladding, and structural material. In order to simplify the heat transfer model of the heat pipe fuel assembly, the irregular shape of the heat pipe fuel assembly is equivalent to the annular region, as shown in Figure 4, in which the ratio of the fuel rod to heat pipe is 3:1 and the axial heat transfer of each layer is neglected. Therefore, the heat conduction equation of the heat pipe fuel assembly is given by:

$$\rho_u C_u \frac{dT_u}{dt} = \frac{1}{r}\frac{\partial}{\partial r}\left(r_u k_u \frac{\partial T_u}{\partial r}\right) + q'''_u + q'''_{cr} \tag{5}$$

where ρ_u is the fuel pellet density (kg/ m^3); C_u is the specific heat of the fuel pellet (J/(kg·K)); T_u is the fuel pellet temperature (K); r_u is the equivalent radius of the fuel assembly (m); k_u is the fuel pellet thermal conductivity (W/(m·K)); and q'''_u is the fuel pellet volume heat

(W/m^3) and q'''_{cr} is the equivalent radial heat transfer between the fuel assemblies, which can be calculated using the solid-core heat transfer model.

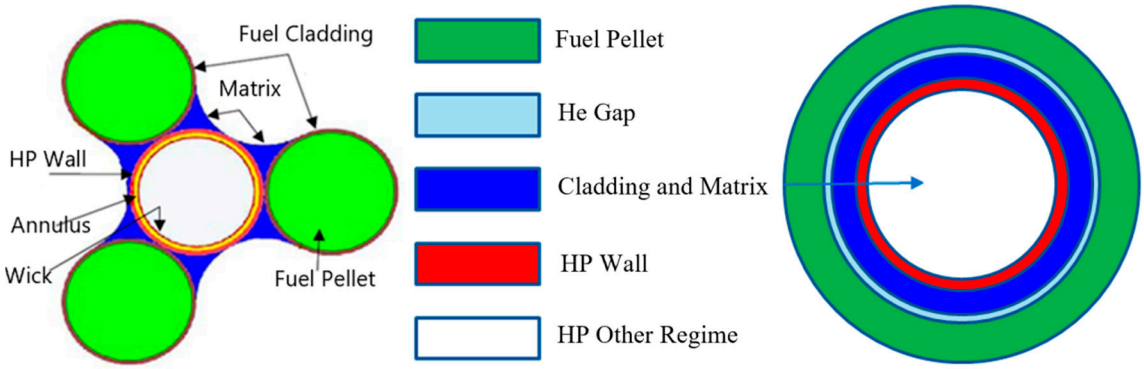

Figure 4. Schematic of equivalent heat transfer model for the heat pipe fuel assembly.

For the fuel cladding and core structural matrix, the temperature is calculated by a 1-D heat conduction equation:

$$\rho_c C_c \frac{dT_c}{dt} = \frac{1}{r}\frac{\partial}{\partial r}\left(r_c k_c \frac{\partial T_c}{\partial r}\right) \tag{6}$$

where ρ_c is the cladding and matrix density (kg/m^3); C_c is the cladding and matrix-specific heat (J/(kg·K)); T_c is the cladding and matrix temperature (K); r_c is the equivalent radius of the fuel assembly (m); and k_c is the cladding and matrix thermal conductivity (W/(m·K)).

The boundary condition between the cladding and heat pipe wall is given by the following formula:

$$-k\frac{\partial T_c}{\partial r}\bigg|_{r=r_m} = h_{hp}\left(T_c - T_{hpe}\right) \tag{7}$$

2.2.3. Equivalent Heat Transfer Coefficient Model

The equivalent heat transfer coefficient between the fuel cladding and heat pipe wall of the HPMR reactor depends on the assembly technology of the heat pipe fuel assembly. For a given HPMR core design, the equivalent heat transfer coefficient h_{hp} at the interface between the fuel cladding and heat pipe wall is usually a certain value. To obtain the heat transfer coefficient, the heat transfer characteristics of the HPMR core are studied under different power and heat pipe wall temperatures by applying Computational Fluid Dynamics (CFD) software. First, the heat flux between the fuel and heat pipe and the temperature of the fuel pellet, fuel gap, structural material, and heat pipe wall can be calculated using CFD software. Thereafter, the equivalent heat transfer coefficient at the interface of the fuel subregion and its adjacent heat pipe is calculated by the average temperature of the structural material and the evaporation section of the heat pipe. For a typical HPMR (such as SAIRS), the equivalent heat transfer coefficient calculated by the CFD software remains unchanged (6995 ± 2 W/(m^2·K)), even if the volume power density of the core fuel and wall temperature of the heat pipe evaporation section are changed, as shown in Figure 5a. Simultaneously, the highest, lowest, and average temperatures of the fuel pellet, air gap, cladding, and subregion structural material (Figure 3) can be corrected by the relationship between the power density of the fuel pellet and the average temperature of the subregion (Figure 5b), which is calculated by using the solid core heat transfer model. Therefore, it is possible to obtain the hot spot temperature of the whole HPMR core.

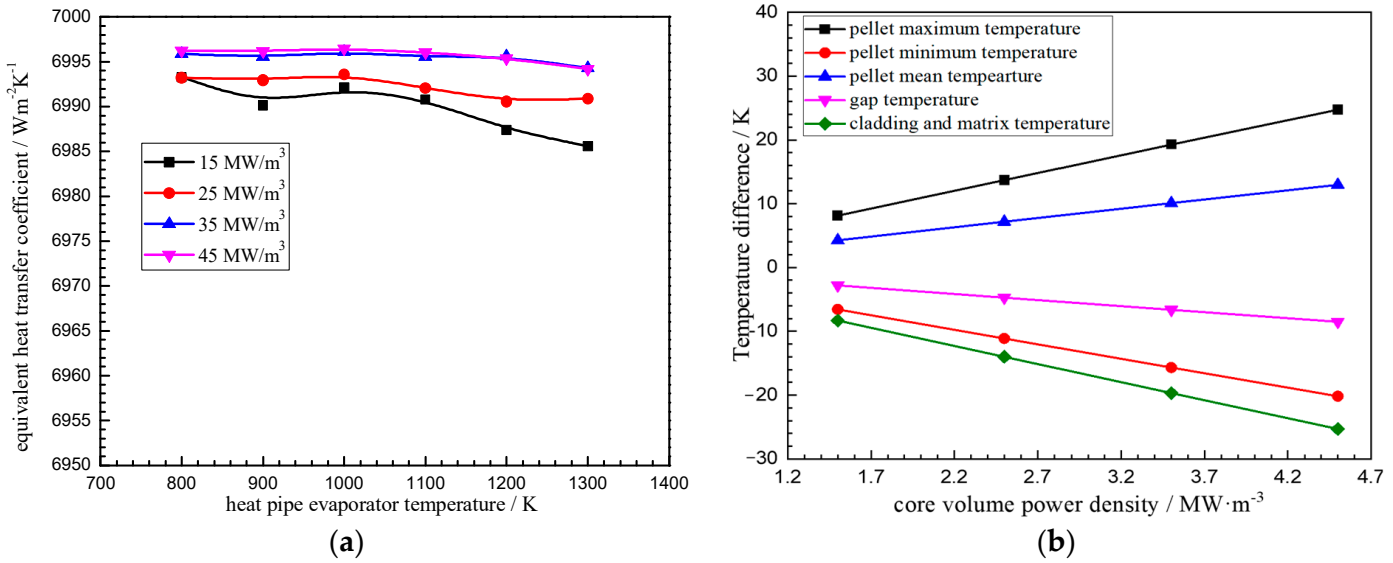

Figure 5. Equivalent heat transfer coefficient model for SAIRS HPMR: (**a**) equivalent heat transfer coefficient and (**b**) temperatures of different fuel materials.

2.3. Heat Pipe Transient Model

The heat pipe transient heat transfer model in the TAPIRS code mainly comprises the thermal resistance network model and flat-front model. However, the heat transfer limit of heat pipe has an important influence on the transient response characteristics of the HPMR system, which has not been considered in the transient heat transfer model of the heat pipe. Therefore, by improving the flat-front model and thermal resistance network model, considering the heat transfer limit of the heat pipe during startup and operation, a heat pipe transient model suitable for the full-stage transient analysis of the HPMR system is established. In this study, the calculation method of the hot zone wall temperature in the flat-front model was revised by dividing the hot zone of the heat pipe into two parts, as shown in Figure 6, so that the heat absorption of the evaporator section and heat transfer of the vapor flow can be considered when the heat pipe reaches the heat transfer limit [18].

$$\begin{aligned} &\text{hot zone 1}: CL_e\frac{dT_{aw,1}}{d\tau} = Q_{in}(\tau) - Q_{\max}(\tau) \\ &\text{hot zone 2}: C\frac{d[(l-L_e)T_{aw,2}]}{d\tau} = Q_{\max}(\tau) - 2\pi q_c r_o(l - L_e - L_a)\delta\tau \end{aligned} \tag{8}$$

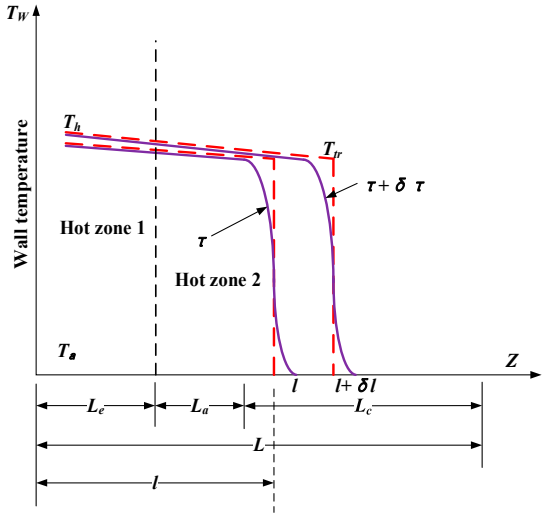

Figure 6. Improved plane-front model considering the heat transfer limit of the heat pipe.

The vapor heat transfer is limited by the heat pipe heat transfer limit $Q_{\max}$. The main heat transfer limits involved in the startup process of the heat pipe are the viscous and sonic limits, which can be obtained by the previously proposed method [25].

The results show that the possible heat transfer limits for continuous flow are capillary limitation, entrainment limitation, and boiling limitation [25]. Similarly, the thermal resistance network model to describe the transient continuous flow of heat pipes was improved by considering the heat transfer limit and expanding to a 2-D multinode thermal resistance model. Additionally, the heat transfer between the evaporator and condenser is determined by solving the temperature gradient equations with a fully 2-D finite difference method.

2.4. Energy Conversion System Model

The TAPIRS code only models the energy conversion system of alkali metal thermoelectric conversion, so it cannot be used to analyze other energy conversion systems designed by new HPMR, such as thermoelectric energy conversion designed by HP-STMC HPSR, Stirling energy conversion of Kilopower, or Brayton energy conversion for Megapower. The TAPIRS code can be improved and extended for advanced HPMR conceptual designs by establishing and integrating a variety of energy conversion system models.

2.4.1. Thermoelectric Conversion Model

For HP-STMC HPSR design, the hot end of thermoelectric (TE) conversion device cells was attached to the condensing sections surface of several core heat pipes, and the cold end of thermoelectric cells was cooled to a lower temperature by the heat pipe radiators. Owing to the Seebeck effect of TE semiconductor materials and the temperature difference between the hot end and the cold end of TE cells, electric power is generated in the thermoelectric cell.

If the physical properties of the TE conversion device cells semiconductor materials are independent of temperature, and the temperatures of TE cells hot end and cold end are constant, the hot end and cold end temperatures of TE cells can be obtained by [26]:

$$\begin{array}{l} K_{TE}(T_{Hend} - T_{Cend}) + \alpha_{pn} T_{Hend} j - 0.5 j^2 (R_P + R_N) = (UA)_{HTE}(T_{HPC,core} - T_{Hend}) \\ K_{TE}(T_{Hend} - T_{Cend}) + \alpha_{pn} T_{Cend} j + 0.5 j^2 (R_P + R_N) = (UA)_{CTE}(T_{Cend} - T_{HPE,radiator}) \end{array} \quad (9)$$

$$j = \frac{\alpha_{pn}(T_{Hend} - T_{Cend})}{R_N + R_P + R_L} \quad (10)$$

where K_{TE} is the effective thermal conductivity of the thermoelectric element (W/K); T_{Hend} and T_{Cend} are the hot end and cold end temperatures of TE cells, respectively (K); α_{pn} is the Seebeck coefficient of TE materials (V/K); j is the TE cell electric current (A); R_P and R_N are the internal electric resistance of the p-type and n-type semiconductor material of the TE cells, respectively (Ω); R_L is the external load resistance (Ω); $(UA)_{HTE}$ and $(UA)_{CTE}$ are the overall equivalent thermal conductivity between a TE cell hot end material and core heat pipe condenser, and that between the cold end material and radiator heat pipe evaporator, respectively (W/K). $T_{HPC,core}$ and $T_{HPE,radiator}$ are the temperatures of the core heat pipe condenser and radiator heat pipe evaporator, respectively (K).

The electric power output P_e is given by:

$$P_e = j^2 R_L \quad (11)$$

The thermal power input to the thermoelectric generator q_{TE} is expressed as:

$$q_{TE} = (UA)_{HTE}(T_{HPC} - T_{Hend}) \quad (12)$$

The efficiency of thermoelectric conversion device η is defined by:

$$\eta = \frac{P_e}{q_{TE}} \tag{13}$$

2.4.2. Stirling Conversion Model

Usually, the Schmidt model is used in Stirling energy conversion analysis of nuclear systems [27]. However, the Schmidt model is an ideal isothermal model, which does not consider heat loss during the cycle. The main assumption of the Schmidt model is that the gas temperature in the expansion and heater spaces is equal to the average constant temperature of the upper source, while the gas temperature in the compression and cooler space is equal to the average constant temperature of the lower heat sink. In order to obtain closed-form solutions, the Schmidt model also assumes that the volume of the workspace changes sinusoidally and the gas mass in the Stirling remains unchanged. Therefore, considering the mechanism of energy loss in Stirling conversion, the equivalent thermal resistance model is used to improve the Schmidt model, as shown in Figure 7.

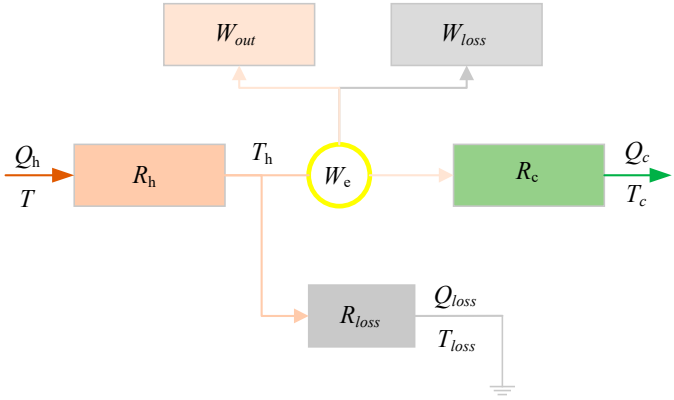

Figure 7. Schematic of Stirling conversion thermal resistance model.

The heat energy Q_h from heat source T is divided into three parts: (1) heat loss Q_{loss} determined by R_{loss} to the environment, (2) work W_e generated from the expansion chamber to the compression chamber, and (3) heat dissipation Q_c through the condensation chamber. Therefore,

$$Q_h = Q_c + Q_{loss} + W_e \tag{14}$$

where W_e is the ideal mechanical output power during a cycle, including the energy loss caused by flow resistance and leakage in gas spaces. Considering the losses,

$$W_e = W_{out} + W_{loss} \tag{15}$$

where W_{out} represents the actual output power, and W_{loss} represents the output power loss. Then, the total conversion efficiency of the Stirling cycle η is defined as:

$$\eta = \frac{(W_e - W_{loss})}{Q_h} \tag{16}$$

For a compact Stirling converter with low power, the internal parameters change very quickly due to high rotating speed, so the Stirling energy conversion system can be in a quasi-steady state at every step of the transient calculation.

2.4.3. Open Brayton Conversion Model

Brayton energy conversion is a type of power conversion system widely used in HPMR design, such as HPMR, a mega power reactor for special purposes. In the MegaPower

design, the evaporation section of heat pipe absorbs heat from the core fuel rods. The condensation section of heat pipe transfers heat to the gas flowing through the intermediate heat exchanger wall. High-temperature gas expands in the turbine, and power is generated through the Brayton open cycle of gas, as shown in Figure 8.

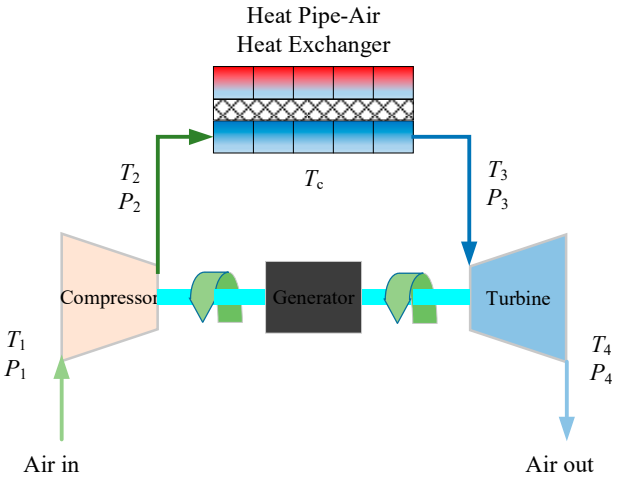

Figure 8. Schematic of simple air Brayton power cycle.

The ambient low-temperature gas is compressed to the optimal pressure by the compressor. Thereafter, the air is heated to the desired temperature by a heat pipe heat exchanger. The high-pressure air gas is expanded through a turbine to generate power. Given the inlet pressure, temperature, and flow rate of air entering the compressor, it is necessary to calculate the equations of outlet temperature and pressure of each component. Therefore, the characteristic curves of the compressor and turbine are used to provide the pressure ratio and efficiency, which are defined as follows:

$$\begin{aligned} \pi_c &= f_1(w,n),\ \eta_c = f_2(w,n) \\ \pi_t &= f_3(w,n),\ \eta_t = f_4(w,n) \end{aligned} \tag{17}$$

where subscript c indicates the compressor, t indicates the turbine, π is the pressure ratio, and η is the isentropic efficiency. According to the known compressor inlet pressure p_1, gas turbine outlet backpressure p_4, and pressure loss coefficient γ, the relationship of the pressure ratio is obtained:

$$p_4\pi_t = \gamma \cdot p_1\pi_c \tag{18}$$

Thereafter, the outlet temperature of the compressor and gas turbine can be calculated by the pressure ratio, isentropic efficiency, and ratio of heat capacities. By simplifying the heat exchanger as a control body and establishing the energy balance equation, the transient change in the gas temperature in the heat exchanger can be obtained:

$$m_c c_p \frac{dT_c}{dt} = Q + \dot{m} c_p (T_2 - T_3) \tag{19}$$

where m_c is the mass of gas in the heat exchanger (kg); T_c is the average temperature of the gas in the heat exchanger (K); and $\dot{m}$ is the mass flow rate of the gas in the heat exchanger (kg/s).

Since the shaft speed varies with the gas flow rate of the turbine, the rotor energy equation is used to determine the shaft speed:

$$\frac{d}{dt}\left(\frac{I\omega^2}{2}\right) = P_t - P_g - P_c \tag{20}$$

where I is the moment inertia of the shaft (kg·m^2); ω is the rotational speed of the shaft; and P_t, P_g, and P_c are the powers generated by the turbine, the power generated by the alternator, and the power consumed by the compressor.

3. Development and Validation of TAPIRSD Code

3.1. Development of TAPIRSD Code

Based on the corresponding differential equations or algebraic equations of each component of the HPMR system, the improved model is solved. For differential equations, such as the fuel assembly heat transfer model, the improved flat-front model for transition flow for heat pipes, and the open Brayton conversion model, the classical fourth-order Runge–Kutta method is probably the most commonly used numerical solution method for these differential equations. For differential-algebraic equations, such as the solid-core heat transfer model and 2-D multinode thermal resistance network model for heat pipes, the Gauss–Seidel iterative numerical solution method is probably the most commonly used numerical solution method for these algebraic equations. In the transient analysis of the HPMR system, they are used to solve the equations of each part in the improved model.

Based on the improved model described above and numerical solution methods, the HPMR transient analysis code TAPIRSD was developed with a modular programming method and FORTRAN language. The TAPIRSD code mainly comprises the main program, global solver module, input and output module, core power module, fuel heat conduction module, heat pipe module, energy conversion module, and waste heat removal module. As shown in Figure 9, the code uses a modular solution process to solve the node temperature from the core fuel to the waste heat removal component in turn at each time step, and corrects the core power by using reactivity feedback and a point kinetics model. TAPIRSD can obtain the heat transfer characteristics of the heat pipe fuel assembly in different regions of the core. The power factor of each region can be provided by user input. The temperature of the fuel assembly can be corrected by solving the heat transfer over the entire core. The improved code can be used to analyze the typical accident conditions of various types of HPMR.

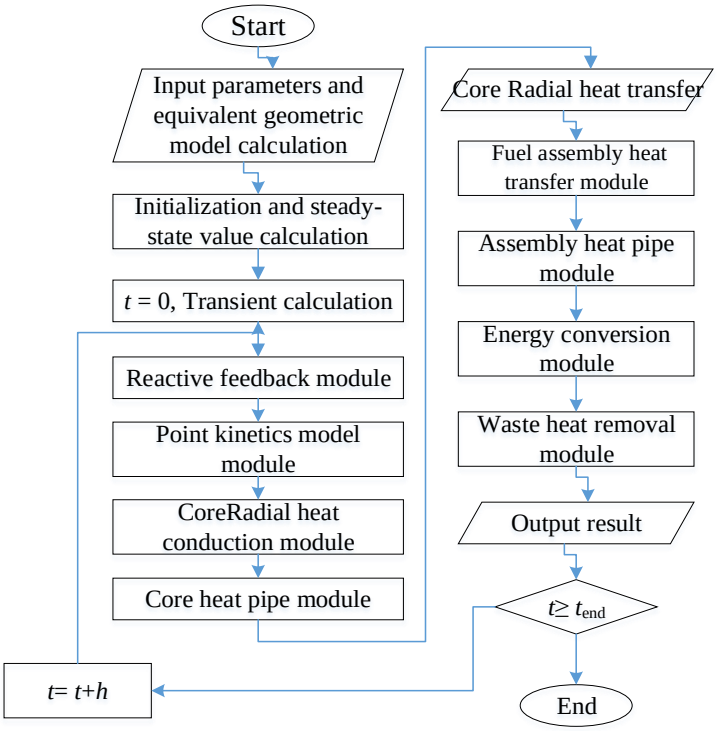

Figure 9. Schematic of TAPIRSD code.

3.2. Validation of Thermoelectric Conversion Model

The thermoelectric conversion model was verified by Wang and Tang's experiments on a TE semiconductor thermoelectric converter [28], which absorbs heat energy from the condensation section of the heat pipe and is cooled by a constant temperature and constant flow water heat exchanger. The calculated results of the model were compared with the experimental results, as shown in Figure 10. For different heat source temperatures of 673, 773, and 873 K, the calculated trend of the output power of the thermoelectric converter with load resistance is in good agreement with the experimental results. When the temperature of the heat source is constant, the output power first increases and then decreases with the increase in load resistance. The maximum relative error between the calculated results and experimental results is less than 8%.

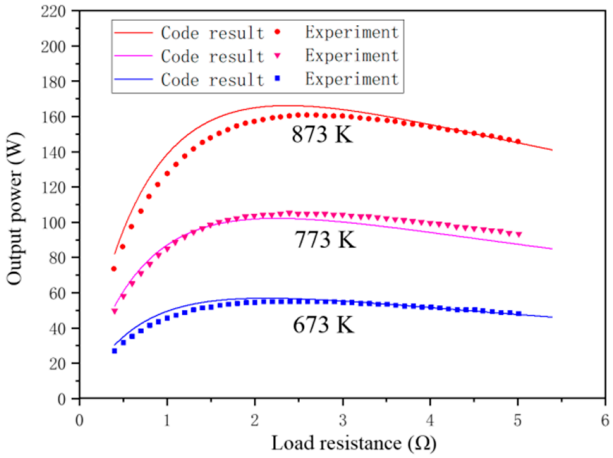

Figure 10. Comparison between the calculated and experimental value of the thermoelectric converter.

3.3. Validation of Stirling Conversion Model

The Stirling conversion model was verified by using the performance test data of the GPU-3 Stirling engine [29]. The performance parameters of GPU-3 under different experimental conditions were analyzed by the TAPIRSD code. The output power of GPU-3 at different heater space average temperatures was calculated and compared with the experimental data in the literature [27], as shown in Figure 11. The calculated results agree well with the test results. The maximum relative error between the calculated results and experimental results is less than 5%, which shows that the model can satisfactorily predict the performance of Stirling conversion.

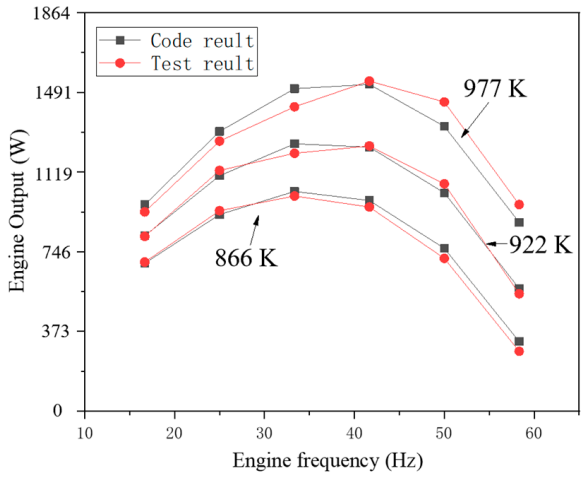

Figure 11. Comparison between the calculated and experimental value of GPU-3 Stirling engine.

3.4. Validation of Open Brayton Conversion Model

Because of the lack of corresponding experimental data of open Brayton conversion, we adopted the SBL-30 Brayton system experiment [30] in Sandia Laboratory to verify the open Brayton conversion model. Assuming the inlet temperature and pressure of the compressor, then the inlet temperature and outlet pressure of the turbine are known. The outlet temperature and pressure of the compressor and the outlet temperature and pressure of the turbine are calculated by using the characteristic flow curves of the SBL-30 compressor and turbine. The calculated results are compared with the SBL-30 experimental results (Figure 12). The results show that the predicted temperature and pressure values agree well with the experimental results, and the maximum temperature error is less than 3%, which proves the accuracy and applicability of the open Brayton conversion model.

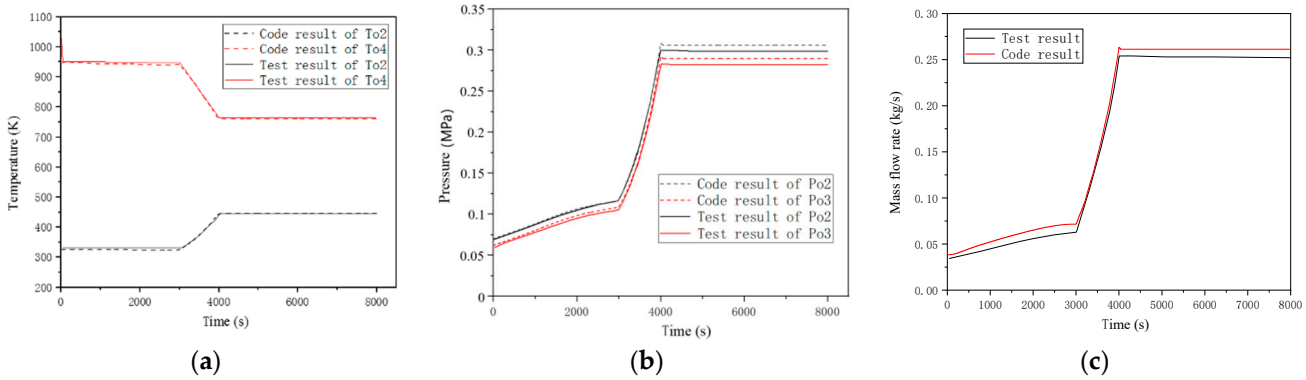

Figure 12. Comparisons between calculated and experimental results of SBL-30 system: (**a**) temperature, (**b**) pressure, and (**c**) mass flow.

4. Validation of TAPIRSD Code with KRUSTY System

The transient safety response of the KRUSTY core, including heat pipe failure, loss of heat sink, and load change accidents, was also analyzed by TAPIRSD. By comparing the calculated results with the published experimental data of the KRUSTY, the accuracy and applicability of TAPIRSD are proved.

4.1. KRUSTY System and Modeling

The KRUSTY reactor [31] is a 1 kW prototype test system using highly enriched uranium as fuel and heat pipe cooling, which is used to demonstrate the design of the Kilopower reactor. In March 2018, KRUSTY was successfully operated as a fission power system. The details of KRUSTY's design together with the general design concepts and methods for all willpower reactors are described in [32]. To test KRUSTY in the vacuum chamber on the Comet, various modifications have been made, but the geometry of the fuel and heat pipe is still very similar to the Kilopower design.

Figure 13 shows the schematic diagram of the integration of KRUSTY and Comet. KRUSTY is an experimental fast reactor cooled by a sodium heat pipe. The design steady-state thermal power is 4 kW, and the output electric power produced by Stirling energy conversion is 1 kW. The reactor core consists of three solid U-7.5 Mo ring fuel elements with an outer diameter (OD) of 11 cm and a total length of 25 cm. The core contains a 4 cm hole, which allows a 10 kW electric heater to be inserted for the non-nuclear test, and a B_4C stack to simulate the flight startup rod during the nuclear test. KRUSTY employs eight sodium heat pipes that transport heat to the Stirling converters and gas-cooled heat dissipation simulators. Specifically, two converters produce electric power and six gas-cooled simulators that used only for heat removal for simulating the actual converters. The inner core is surrounded by multilayer molybdenum insulation materials and a 316 stainless-steel (SS 316) vacuum tank. The neutron reflector of KRUSTY is BeO. All sides of the KRUSTY reactor are shielded; its radial shield is made of type 304 stainless-steel

(SS 304), and its axial shield is made of B_4C and SS 304. The main parameters of the KRUSTY reactor are shown in Table 1.

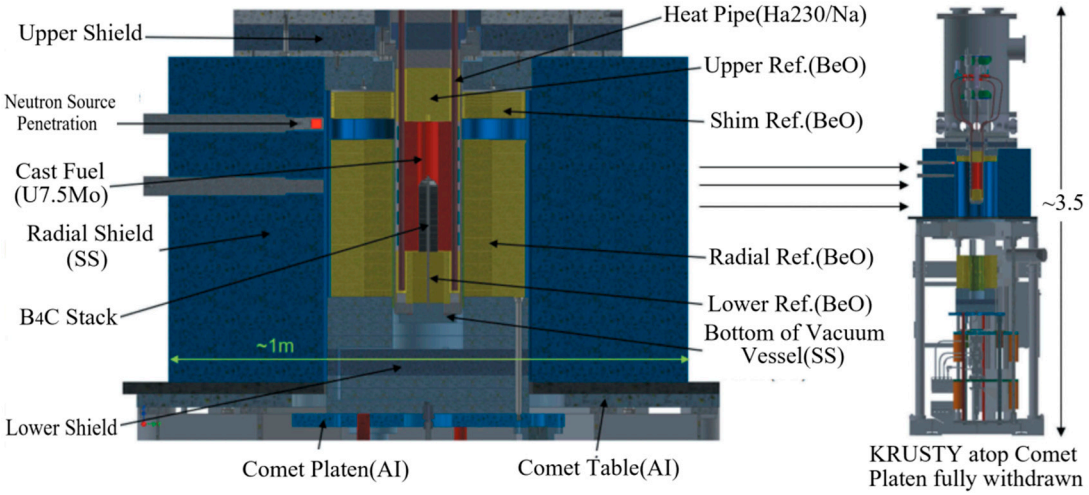

Figure 13. KRUSTY reactor configuration [31].

Table 1. The main design parameters of the KRUSTY reactor.

Parameters	Value	Parameter	Value
Core diameter	11 cm	Heat pipe number	8
Core height	25 cm	Working fluid	Sodium
Total fuel mass	32.20 kg	Operating temperature	990–1073 K
B_4C control rod diameter	4 cm	Outside diameter	1.27 cm
Maximum thermal power	5 kW	Wall thickness	0.089 cm
Nominal thermal power	3 kW	Evaporation length	35.6 cm
Output power	1 kWe	Adiabatic length	86.4 cm
Average core temperature	1073 K	Condenser length	8.89 cm
Core heat loss	400~500 W	Wall material	Haynes 230
Fuel material	U-7.5 Mo	Wick material	Stainless 316
Mo mass fraction	7.8%	Condenser average temperature	~1048 K
U^{235} enrichment	93.1%	Stirling machines number	2 + 6 Simulators
Temperature reactivity coefficient	−0.002 $/K	Stirling type	ASC E2-7, E2-8

The analysis model of the KRUSTY reactor was established by using TAPIRSD. The temperature negative feedback effect of fuel, reflector, and heat pipe was considered in the core power model. The total negative feedback coefficient of temperature is about –0.002 $/K. In KRUSTY's 28 h experiment, the temperature drift during the experiment was taken into account in the TAPIRSD analysis model. Because the reactor BeO reflector was continuously heated, it could not reach a steady state. The heating rate of the reflector was 1 K/h, while the external reactivity remained unchanged. Table 2 gives the physical parameters of the KRUSTY reactor in the core power model.

Table 2. Neutron physical parameters in the KRUSTY core.

Group Number	Delayed Neutron Effective Fraction	Decay Constant (1/s)
1	0.037	0.01273
2	0.211	0.03175
3	0.187	0.116
4	0.407	0.3118
5	0.131	1.399
6	0.027	3.876

KRUSTY core is radially divided into three areas by the TAPIRSD code: control rod, core fuel, and heat pipe. As shown in Figure 14, the core is divided into eight equal parts along the circumference, which is equivalent to eight core heat pipes. The control rod area is divided into two radial control volumes. The core fuel is divided into three radial control volumes. The radial equivalent diameter of the control volume was calculated based on the area weight. The boundary between the fuel zone and heat pipe is set to be equivalent convection heat transfer. There is a vacuum insulation layer between the core layer and the reflector, so the heat dissipation from the core layer to the reflector is small. The equivalent heat loss from the core is assumed as the internal heat source of the outermost fuel control volume.

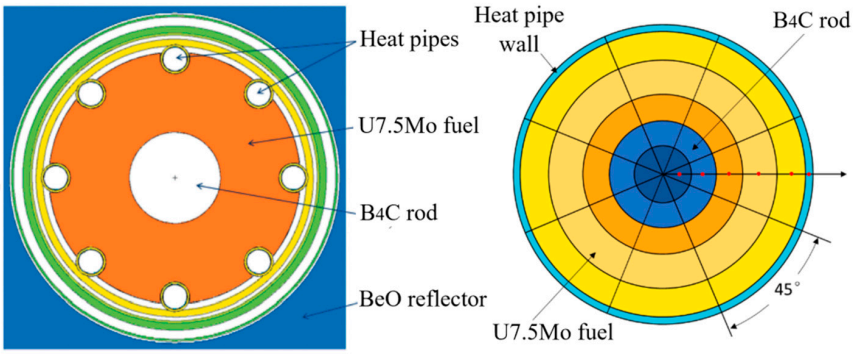

Figure 14. KRUSTY reactor core heat transfer model: (**a**) reactor core and (**b**) core model.

Although the structure of the KRUSTY core heat pipe is different from traditional HTHP, their transient working mechanism is the same. Therefore, the KRUSTY heat pipe model can be transformed into a three-layer, wall–liquid annulus–wick model of a traditional HTHP according to the volume equivalent. Because of the lack of parameters of the Stirling convertor and simulator in the published experimental results, the experimentally measured cooling capacity of the simulator is used as the boundary condition of energy conversion.

4.2. Heat Pipe Failure Accident

In the experimental test of the KRUSTY system, the system characteristics of heat pipe failure were tested during t = 12.0 ~ 14.0 h. At t = 12.0 h, the N_2 flow of the simulator connected to the heat pipe at a 0 deg azimuth of core was cut to simulate the failure of the corresponding heat pipe. Because of the failure of the zero-flow heat pipe, the heat dissipation power decreased from about 290 W to about 120 W. When t = 12.5 h, the N_2 flow of the other simulators increases to provide the power needed to generate the nominal electric power. The temperature on the core surface at 45 and 180 deg were recorded in the test and the reactor core fission power. The TAPIRSD code was used to simulate the transient response characteristics of KRUSTY. The calculation results are compared with the experimental data, as shown in Figure 15.

The measured temperature distribution on the circumferential surface of the core is uneven, which was not considered in the TAPIRSD code. The initial steady state at the two locations of different angles is the same and assumed to be the average experimental measured temperatures at the two locations, as shown in Figure 15b. As the N_2 flow to the simulator at the 0 deg azimuth was cut, the heat transfer power of the heat pipe also decreased rapidly, indicating that the transient failure accident of the heat pipe had occurred. Therefore, the heat generated in the core region where the heat pipe failed can only be discharged by other heat pipes in the adjacent region. Therefore, the local surface temperature of the adjacent 45-degree core increased. At the same time, due to the negative feedback effect of fuel, the total fission power of the core decreases. Therefore, the surface temperature of the core at 180 deg decreases due to the decrease in rector power, which

makes the core circumferential temperature distribution more uneven. When the N_2 flow rate of the other simulators increases to provide the power required for nominal electrical power at t = 12.5 h, the temperature in the normal core area decreases and the total fission power of the core increases, which is due to the negative fuel feedback effect leading to the local temperature increase in the core failure zone.

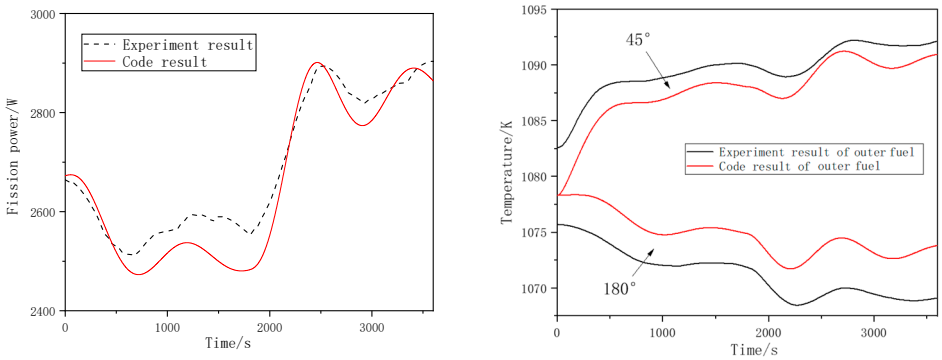

(**a**) (**b**)

Figure 15. Core power and temperature at the heat pipe failure accident: (**a**) core power and (**b**) temperature.

According to this analysis, KRUSTY's heat pipe failure accident leads to a more uneven distribution of power and temperature in the core. The calculated values of transient response trends of the core power and temperature agree well with the measured values. The maximum temperature error is less than 10 K.

4.3. Load Change Transient Conditions

In the experiment of KRUSTY, at t = 8.0 h, the coolant mass flow rate of the air-cooled simulator was reduced by half and the cooling power of each simulator decreased from 290 W to about 210 W. At t = 9 h, the cooling power of the air-cooled simulator returned to be normal and the reactor recovered to the initial steady-state condition with the fission power of 2.75 kW. Then, at t = 10.02 h, the coolant mass flow rate of the air-cooled simulator double. The cooling power of each simulator increased from 295 W to about 510 W. As mentioned above, the transient conditions of reducing and increasing load power are all carried out by experiments, and are also simulated and analyzed by using the TAPERED code. The calculated results of KRUSTY core power and temperature are in good agreement with the experimental data, as shown in Figures 16 and 17.

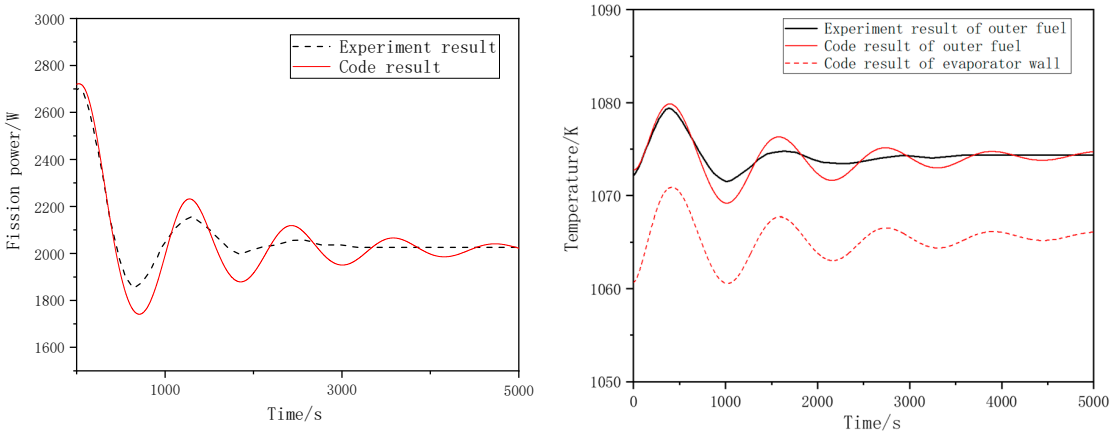

(**a**) (**b**)

Figure 16. Core power and temperature variation under load decreasing condition: (**a**) core power and (**b**) core temperature.

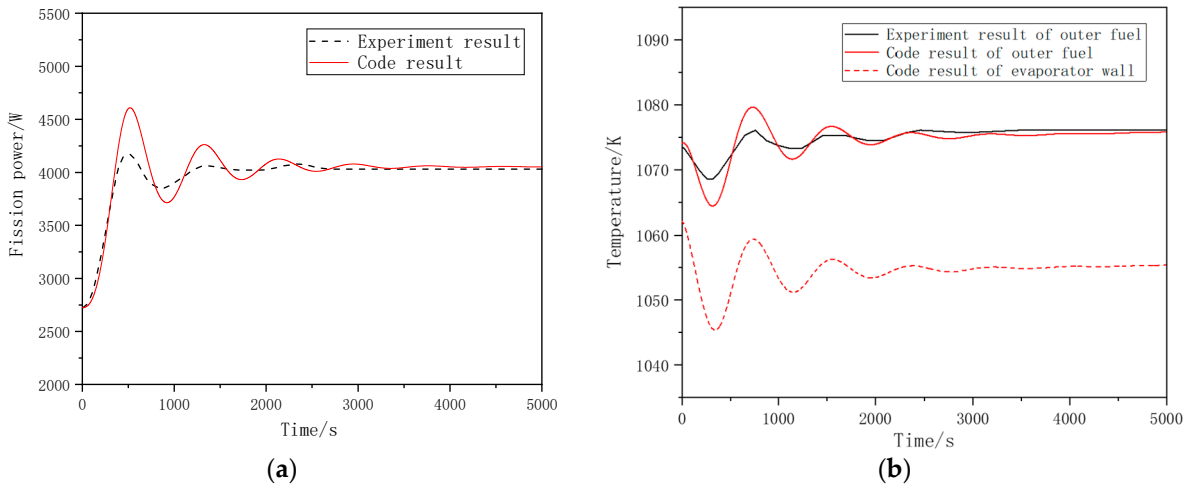

Figure 17. Core power and temperature variation under load increasing condition: (**a**) core power and (**b**) core temperature.

The decrease in load (cooling power) leads to the increase in the average temperature of the reactor core and heat pipe wall, which reduces the reactivity (mainly through the negative feedback effect of the fuel) and finally leads to the decrease in reactor power. Subsequently, the gradual decrease in reactor power caused the average temperature of the reactor core and heat pipe wall to fall back to the set value of the reactor thermostat of about 1073 K, as shown in Figure 16. When the power was at its peak, the temperatures approach their set point at a maximum rate of increase. When power reaches its nominal value at the maximum drop rate, the temperature reaches its peak. The results predicted by the TAPIRSD code are very consistent with those measured by the experiment, which proves the accuracy of the TAPIRSD code and the improved model. It can be seen in Figure 17 that the transient response of the KRUSTY reactor under the operation condition of increasing load is opposite to those under the operation condition of decreasing load. By comparing with the experimental data, the simulation results agree well with the experimental measurement results. Although the temperature oscillation amplitude is larger than the measured data, the calculated results of the TAPIRSD code are consistent with the experimental data, especially the errors of the peak and valley value, which are less than 2%.

4.4. Loss of Heat Sink Accident

For the KRUSTY experiment when t = 20 h, the Stirling converters were stalled (zero strokes) and the simulator flow was set to a very low rate, which was conducted to simulate a complete loss of active heat removal of KRUSTY. In this experimental condition, the steady-state power of the reactor decreased from 2.6 to 1.5 kW and the average cooling power of the heat pipe condenser decreased from about 270 to 130 W. The loss of heat sink accident was analyzed by TAPIRSD and the transient response characteristics of KRUSTY are shown in Figure 18.

After cutting off the flow rate of the simulator, the core temperature increased quickly, causing the reactivity and power to drop quickly. Finally, a new steady-state power that matched the cooling power was achieved. The calculated temperature at the outer surface of fuel increased by about 4 K within 2 h. This occurred because the radial temperature gradient of fuel was small at a lower power level. The temperature of the inner and outer fuel and the heat pipes would become close to the average temperature, which is consistent with the experimental results.

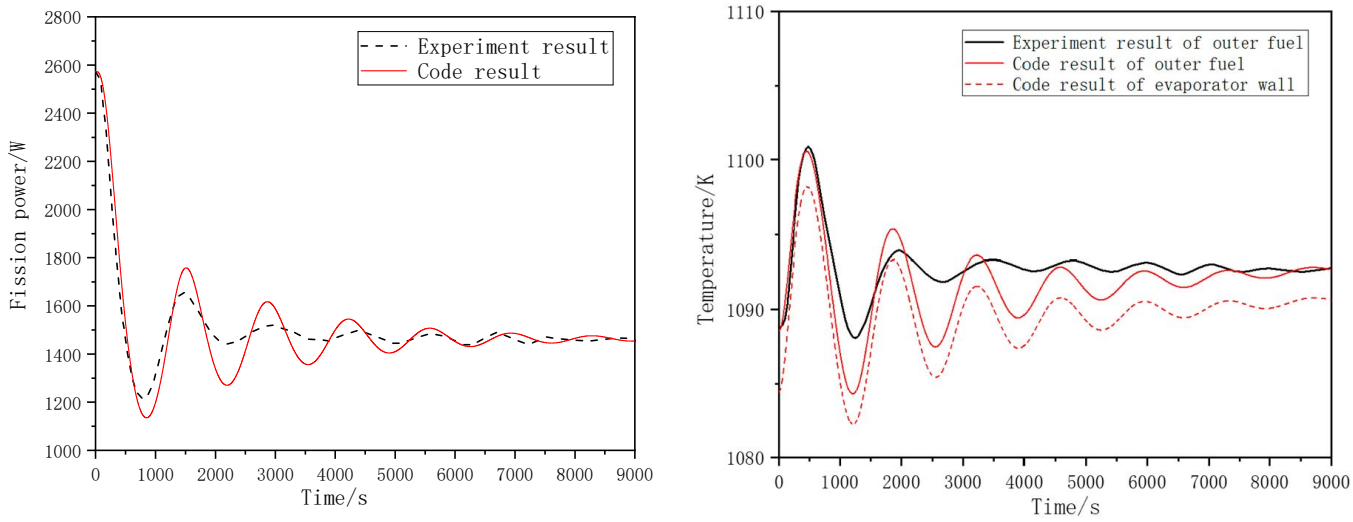

Figure 18. Core power and temperature for the loss of heat sink accident: (**a**) core power and (**b**) temperature.

5. Conclusions

HPMR is considered a multifunctional and reliable solution, which can solve some special power supply challenges in various military and civil applications. The potential customer of HPMRs' power and heat include high-power communication stations, frontier or remote operation bases, isolated microgrid communities, expeditionary or permanent military bases, and offshore isolated platforms. HPMR is also considered as a supermobile response option to manage natural disasters and other infrastructure disruptions. To analyze and evaluate the transient safety response characteristics of HPMRs under accident conditions, including the failure of the heat pipe in the core and the loss of system heat sink and other accidents, an improved model based on a previously developed transient analysis model for HPSRs was established. The following conclusions were drawn.

(1) The radial two-dimensional heat conduction model of all-solid core can be used for the core heat pipe failure and system heat sink loss accidents. Using the equivalent heat transfer coefficient between the fuel and heat pipe, the maximum temperature of the fuel in this subregion can be calculated, and the safety characteristics of the HPMR can be studied.

(2) The conversion system models include thermoelectric conversion, Stirling conversion, and open Brayton conversion to simulate the system characteristics of the advanced HPMR concept. The maximum deviation of the power output predicted by the energy conversion model is less than 8%.

(3) Based on these models, the HPMR system analysis code TAPIRSD was developed and validated by experimental data of the ground prototype device KRUSTY of the Kilopower space reactor. Although the temperature oscillation amplitude is larger than the measured data, the calculated results of the TAPIRSD code are consistent with the experimental data, especially the errors of the peak and valley value, which are less than 2%, demonstrating the accuracy and reliability of the improved model and code.

(4) The improved transient analysis model and code of the HPMR system in this paper can be used in the future for transient safety analysis and design optimization of the different kinds of HPMR systems.

Author Contributions: Conceptualization, L.G. and H.L.; methodology, H.L. and Z.O.; validation, Z.O., H.L. and L.G.; formal analysis, X.K.; investigation, H.L.; resources, D.L.; data curation, Z.O.; writing—original draft preparation, H.L.; writing—review and editing, X.T. and L.G.; visualization, X.K.; supervision, J.S. and X.J.; project administration, X.J.; funding acquisition, J.S. All authors have read and agreed to the published version of the manuscript.

Funding: This research was supported by the National Key R&D Program of China [Grant No. 2018YFB190064] and National Natural Science Foundation of China [Grant No. 12005162].

Institutional Review Board Statement: Not applicable.

Informed Consent Statement: Not applicable.

Data Availability Statement: Not applicable.

Acknowledgments: The authors would like to thank deeply to the anonymous reviewers for their constructive comments on this paper.

Conflicts of Interest: The authors declare no conflict of interest.

List of Symbols

Nomenclature

C_p	specific heat (J/(kg·K))
T	temperature (K)
V	volume (m^3)
t	time (s)
L	heat pipe length (m)
r	radius (m)
k	thermal conductivity (W/(m·K))
Q	power (W)
N	number of heat pipes (-)
h	heat transfer coefficient (W/ (m^2·K))
A	heat transfer area (m^2)
q'''	volume power density (W/m^3)
K	thermal conduction (W/K)
L	length (m)
R	electric resistance (Ω)
UA	overall thermal transfer (W/K)
j	electric current (A)
P	electric power (W)
W	mechanical output power (W)
m	gas mass (kg)
I	moment inertia of shaft (kg·m)
p	pressure (Pa)

Greek symbols

ρ	density (kg/m^3)
α	Seebeck coefficient (V/K)
η	efficiency of thermoelectric conversion or isentropic efficiency
π	pressure ratio
γ	pressure loss coefficient
ω	speed of shaft

Subscripts

a	heat pipe adiabatic section
max	heat pipe heat transfer limitation
f	fuel
hp	heat pipe
hpe	heat pipe evaporation section
u	fuel pellet
c	cladding and matrix or condenser surface
aw	average temperature of wall
pn	p-type and n-type

References

1. Sterbentz, J.W.; Werner, J.E.; McKellar, M.G.; Hummel, A.J.; Kennedy, J.C.; Wright, R.N.; Biersdorf, J.M. *Special Purpose Nuclear Reactor (5 MW) for Reliable Power at Remote Sites Assessment Report*; INL/EXT-16-40741; Idaho National Lab.: Idaho Falls, ID, USA, 2017.
2. Allen, K.S.; Hartford, S.K.; Merkel, G.J. Feasibility Study of a Micro Modular Reactor for Military Ground Applications. *J. Def. Manag.* **2018**, *8*, 172. [CrossRef]
3. Smith, C.F.; Halsey, W.G.; Brown, N.W.; Sienicki, J.J.; Moisseytsev, A.; Wade, D.C. *SSTAR: The U.S. Lead-Cooled Fast Reactor (LFR)*; URL-JRNL-235075; Lawrence Livermore National Laboratory: Livermore, CA, USA, 2007.
4. Dasari, V.R.; Trellue, H.R.; Arafat, Y. *Microreactors: A Technology Option for Accelerated Innovation*; LA-UR-20-22435; Los Alamos National Laboratory: Los Alamos, NM, USA, 2020.
5. Nazari, M.A.; Ahmadi, M.H.; Ghasempour, R.; Shafii, M.B.; Mahian, O.; Kalogirou, S.; Wongwises, S. A review on pulsating heat pipes: From solar to cryogenic applications. *Appl. Energy* **2018**, *222*, 475–484. [CrossRef]
6. Wang, D.; Guo, Y. Preliminary Design of a Heat Pipe-Cooled Blanket for CFETR. *Energies* **2021**, *14*, 6879. [CrossRef]
7. Nazari, M.A.; Ahmadi, M.H.; Sadeghzadeh, M.; Shafii, M.B.; Goodarzi, M. A review on application of nanofluid in various types of heat pipes. *J. Cent. South Univ.* **2019**, *26*, 1021–1041. [CrossRef]
8. Gibson, M.A.; Oleson, S.R.; Poston, D.I.; McClure, P. NASA's Kilopower Reactor Development and the Path to Higher Power Missions. In Proceedings of the 2017 IEEE Aerospace Conference, Big Sky, MT, USA, 4–11 March 2017.
9. Arafat, Y.; van Wyk, J. Vinci™ Micro Reactor. *Nucl. Plant J.* **2019**, *37*, 34–36.
10. Mireles, O.R.; Houts, M.G. Transient Response to Rapid Cooling of a Stainless-Steel Sodium Heat Pipe. In Proceedings of the Nuclear and Emerging Technologies for Space 2011, Albuquerque, NM, USA, 7–10 February 2011.
11. Wright, S.A.; Houts, M. Coupled Reactor Kinetics and Heat Transfer Model for Heat Pipe Cooled Reactors. *AIP Conf. Proc.* **2001**, *552*, 815–821.
12. Poston, D.I.; Dixon, D.D.; Marcille, T.F.; Benjamin, W. Amiri. FRINK—A Code to Evaluate Space Reactor Transients. *AIP Conf. Proc.* **2007**, *880*, 449.
13. Ge, L.; Li, H.; Shan, J. Reliability and loading-following studies of a heat pipe cooled AMTEC conversion space reactor power system. *Ann. Nucl. Energy* **2019**, *130*, 82–92. [CrossRef]
14. Zhang, H.; Ye, F.; Guo, H.; Yan, X. Isothermal Performance of Heat Pipes: A Review. *Energies* **2022**, *15*, 1992. [CrossRef]
15. Zhang, H.; Ye, F.; Guo, H.; Yan, X. Sodium-Potassium Alloy Heat Pipe under Geyser Boiling Experimental Study: Heat Transfer Analysis. *Energies* **2021**, *14*, 7582. [CrossRef]
16. Sun, H.; Tang, S.; Wang, C.; Zhang, J.; Zhang, D.; Tian, W.; Qiu, S.; Su, G. Numerical simulation of a small high-temperature heat pipe cooled reactor with CFD methodology. *Nucl. Eng. Des.* **2020**, *370*, 110907. [CrossRef]
17. Wang, C.; Duan, Q.; Liu, M.; Zhang, D.; Qiu, S.; Su, G.; Tian, W. Code development and analysis of heat pipe cooled passive residual heat removal system of Molten salt reactor. *Ann. Nucl. Energy* **2020**, *144*, 107527. [CrossRef]
18. Li, H.; Ouyang, Z.; Tian, X.; Ge, L.; Li, D.; Kang, X.; Shan, J. The development of high temperature heat-pipe transient model for system analysis of heat pipe cooled microreactor. *Prog. Nucl. Energy* **2022**, *146*, 104115.
19. El-Genk, M.S.; Tournier, J.-M. Conceptual Design of HP-STMC Space Reactor Power System for 110-kWe. 10-Year Mission. In *These Proceedings of Space Technology and Applications International Forum (STAIF-04)*; El-Genk, M.S., Ed.; American Institute of Physics: Melville, NY, USA, 2004.
20. Li, H.; Tian, X.; Ge, L.; Kang, X.; Zhu, L.; Chen, S.; Chen, L.; Jiang, X.; Shan, J. Development of a Performance Analysis Model for Free-Piston Stirling Power Convertor in Space Nuclear Reactor Power Systems. *Energies* **2022**, *15*, 915. [CrossRef]
21. Poston, D.I.; Gibson, M.A.; Sanchez, R.G.; McClure, P.R. Results of the KRUSTY nuclear system test. *Nucl. Technol.* **2020**, *206* (Suppl. S1), S89–S117. [CrossRef]
22. Gibson, M.A.; Poston, D.I.; McClure, P.R.; Sanzi, J.L.; Godfroy, T.J.; Briggs, M.H.; Wilson, S.D.; Schifer, N.A.; Chaiken, M.F.; Lugasy, N. Heat Transport and Power Conversion of the Kilopower Reactor Test. *Nucl. Technol.* **2020**, *206* (Suppl. S1), 31–42. [CrossRef]
23. Yuan, Y.; Shan, J. Accident analysis of heat pipe cooled and AMTEC conversion space reactor system. *Ann. Nucl. Energy* **2016**, *94*, 706–715. [CrossRef]
24. El-Genk, M.S.; Tournier, J.-M. "SAIRS"—scalable AMTEC integrated reactor space power system. *Prog. Nucl. Energy* **2004**, *45*, 25–69. [CrossRef]
25. Li, H.; Jiang, X.; Chen, L.; Yang, N.; Zhang, L. Analysis of heat transfer capability of space reactor heat pipe. *At. Energy Sci. Technol.* **2015**, *1*, 89–95.
26. Seo, J.T.; El-Genk, M.S. *Analysis of the Transient Behavior of Thermoelectric Generators. Space Nuclear Power Systems 1986 CONF-860102*; Orbit Book Company: London, UK, 1987; pp. 187–198.
27. Regan, T.; Lewandowski, E. Development of a Linear Stirling System Model with Varying Heat Inputs. In Proceedings of the 5th International Energy Conversion Engineering Conference and Exhibit (IECEC), St. Louis, MO, USA, 25–27 June 2007.
28. Tang, S.; Wang, C.; Liu, X.; Su, G.; Tian, W.; Qiu, S.; Zhang, Q.; Liu, R.; Bai, S. Experimental investigation of a novel heat pipe thermoelectric generator for waste heat recovery and electricity generation. *Int. J. Energy Res.* **2020**, *44*, 7450–7463. [CrossRef]
29. Thieme, L.G. *Low-Power Baseline Test Results for the GPU-3 Stirling Engine*; NASA-TM-1979-79103; U.S. Department of Energy, Office of Conservation and Solar Applications, Division of Transportation Energy Conservation: Columbus, OH, USA, 1979.

30. Wright, S.A.; Lipinski, R.J.; Vernon, M.E.; Sanchez, T. *Closed Brayton Cycle Power Conversion Systems for Nuclear Reactors*; Technical Report; Sandia National Lab.: Albuquerque, NM, USA, 2006.
31. Poston, D.I.; Gibson, M.A. Thomas Godfroy & Patrick R.McClure KRUSTY Reactor Design. *Nucl. Technol.* **2020**, *206*, 13–30.
32. McClure, P.R.; Poston, D.I.; Gibson, M.A. Kilopower Project: The KRUSTY Fission Power Experiment and Potential Missions. *Nucl. Technol.* **2020**, *206*, S1–S12. [CrossRef]